PCCP

Accepted Manuscript

ROYAL SOCIETY OF CHEMISTRY

www.rsc.org/pccp

Table of Contents Entry

From (Au_5Sn + AuSn) physical mixture to phase pure AuSn and Au_5Sn intermetallic nanocrystals with tailored morphology: digestive ripening assisted approach

Neha Arora[a] and Balaji R. Jagirdar*[a]

Digestive ripening facilitated interatomic diffusion has been exploited for the phase controlled synthesis of homogeneous intermetallic nanocrystals of Au-Sn system with a tailored morphology.

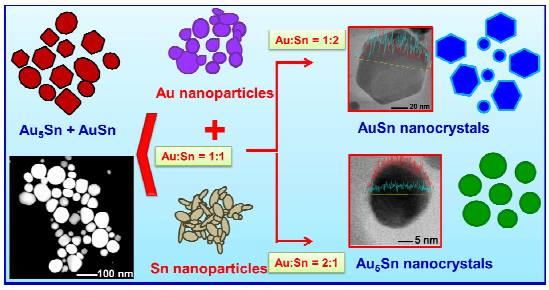

Cite this: DOI: 10.1039/c0xx00000x

www.rsc.org/xxxxxx

ARTICLE TYPE

From (Au_5Sn + AuSn) physical mixture to phase pure AuSn and Au_5Sn intermetallic nanocrystals with tailored morphology: digestive ripening assisted approach

Neha Arora[a] and Balaji R. Jagirdar*[a]

Received (in XXX, XXX) XthXXXXXXXXX 20XX, Accepted Xth XXXXXXXXX 20XX
DOI: 10.1039/b000000x

Here we present digestive ripening facilitated interatomic diffusion for the phase controlled synthesis of homogeneous intermetallic nanocrystals of Au-Sn system. Au and Sn metal nanoparticles synthesized by solvated metal atom dispersion (SMAD) method are employed as precursors for the fabrication of AuSn and Au_5Sn which are Au-rich Au-Sn intermetallic nanocrystals. By optimizing the stoichiometry of Au and Sn in the reaction mixture, and by employing the growth directing agents, the formation of phase pure intermetallic AuSn and Au_5Sn nanocrystals could be realized. The as-prepared Au and Sn colloidal nanoparticles and the resulting intermetallic nanocrystals are thoroughly characterized by powder X-ray diffraction, transmission electron microscopy (TEM and STEM-EDS), and optical spectroscopy. The results obtained here demonstrate the potential of solution chemistry which allows synthesizing phase pure Au-Sn intermetallics with a tailored morphology.

Introduction

Intermetallic nanomaterials wield immense scientific leverage as they exhibit complementary novel physical and chemical properties owing to the synergistic effects among its constituent metals.[1,2] Due to the structural and compositional diversities, these materials are considered as desired candidates in myriad of applications including catalysis,[3] optoelectronic,[4] and hydrogen storage.[5] The dimensions, morphology, phase, atomic distribution, and chemical composition are all pertinent parameters which dictate the properties of intermetallic nanostructures. Hence, achieving a rational control over phase as well as morphology of intermetallic nanostructures has become an intriguing area of interest. The phase and shape-controlled synthesis of intermetallic materials in nano-dimensions has been documented in the literature.[6,7] Schaak and co-workers pioneered the low-temperature solution chemistry approach by adopting "conversion chemistry" towards the synthesis of various intermetallic nanostructures.[8]

Here we have chosen Au-Sn based intermetallics which possess intriguing electronic properties and have displayed promising technological applications in electronic packaging industries such as lead-free solders. Sn based alloys are enticing soft solders and on a rise as interconnect materials in optoelectronic devices due to their environmental benign nature.[9] Specifically, Au-rich Au/Sn alloys are suitable materials in optoelectronic industries owing to their excellent fatigue resistance, creep resistance, long-term device reliability and excellent thermal and electrical conductivities.[10] An important prerequisite for high quality electronic manufacturing is to have a solder with low re-flow temperature.[11] As is known, miniaturization of bulk solders with controlled phase and morphology can be effectively used to bring down their melting temperature.[12]Au-Sn intermetallics also exhibit superconductivity at a low temperature of 1.92 K.[13] The equilibrium phase diagram of Au-Sn binary system is an entrancing subject for researchers and has been studied widely under bulk-scale equilibrium conditions.[13,14] Au-Sn binary system stabilizes in four different intermetallic compounds such as, Au_5Sn (ζ), AuSn (δ), $AuSn_2$ (ε), and $AuSn_4$ (η). Au_5Sn and AuSn intermetallic compounds constitute a eutectic Au-Sn alloy composition (29 at.% Sn) with comparatively low melting temperature of 278 °C. Because of which, they exert leverage over other hard solders in temperature sensitive applications. Au_5Sn has a close-packed hexagonal structure with the unit cell of super structure containing 15 Au and 3 Sn atoms. It has a composition of 16.7 at.% Sn and a homogeneity range of less than 1 at.% Sn.[15] The structure of the AuSn lattice is NiAs-type hexagonal with two molecules of AuSn associated with the unit cell and has a homogeneity range between 50.0 and 50.5 at.% Sn.[16] In comparison to AuSn, Au_5Sn nanocrystals are relatively less explored.

Au-Sn bimetallic architectures have been largely fabricated as thin films. Ivey and co-workers described the fabrication of Au rich, Au-Sn alloy in thin film form by sequential electrodeposition and reflow process at 320-350 °C.[17] They found that the variation in deposition current density can be used to plate two different phases of Au-Sn system.[18] Wang *et al.* observed the nucleation of AuSn and $AuSn_4$ intermetallic phase during inter-diffusion process across the junction in Au/Sn/Au nanowires synthesized by a template electrodeposition method.[19] In comparison to metallurgical techniques which have been

commonly employed for the fabrication of intermetallics, solution based methods have been shown to be beneficial. It eliminates the solid-solid diffusion as the rate limiting step and thus leaves the use of high temperature annealing superfluous. Interatomic diffusion at nanoscale dimensions gives better control over size, crystallinity, and morphology. The resulting intermetallic nanoparticles have high dispersion due to which they can be functionalized easily. Also, it has been shown that these well-formed intermetallic nanocrystals can be used as precursors for the formation of core/shell nanocomposite catalysts.[20,21] To the best of our knowledge, reports on solution synthesis of Au-rich Au-Sn intermetallics phase formation in nanometer-sized particles are very limited.[22] Cable and Schaak described the low-temperature solution synthesis of Au_5Sn intermetallic nanocrystals using polyol process.[8a] Tabatabaei *et al.* reported the formation of AuSn nanoparticles by chemical reduction method.[11]

Herein, we present the synthesis of Au-Sn intermetallic colloidal nanocrystals using digestive ripening assisted process.[23] Digestive Ripening termed as a "temperature dependent size modification" process involves the transformation of a polydisperse colloid into a monodisperse colloid by heating at or near the boiling point of the solvent in the presence of a surface-active ligand. This size variation process involves the digestive ripening agent assisted mass transfer from one particle to another at atomic scale until a dynamic equilibrium in the particle size is achieved. This process has been efficaciously utilized for the synthesis of highly monodisperse metal,[24] semiconductors,[25] core shell,[26] alloy,[27] and intermetallic nanoparticles.[28]

Typically, our methodology involves two steps; firstly gold and tin colloids are synthesized by the solvated metal atom dispersion (SMAD) method.[29] Subsequently two colloids, mixed in a stoichiometric amount are subjected to digestive ripening process which gradually leads to the formation of phase controlled Au-Sn intermetallic nanocrystals. The structural and morphology evolution are systematically studied using a combination of techniques like UV-visible spectroscopy, powder X-ray diffraction, TEM, HRTEM, and STEM-EDS mapping. As-prepared intermetallic nanocrystals obtained are homogeneous therefore, such an approach eliminates the use of high temperature annealing treatment. Solution annealing together with digestive ripening process leads to the formation of intermetallic nanocrystals from pre-synthesized monometallic nanoparticles with a precise control on their phase and morphology. Also, this methodology obviates the use of strong reducing agents and renders the approach facile. We envisage that this technique can also be employed for synthesizing monodisperse nanocrystals of various intermetallic systems.

Results and discussion

1. Au-nanoparticles synthesized in THF

THF as a coordinating solvent and stabilizing agent produced dark violet colored Au colloids. The UV-visible absorption spectrum recorded for Au-THF colloid exhibited a broad SPR band centered at 580 nm, indicative of polydispersion in size (Fig. 1a). The nature of the Plasmon absorption band is known to depend upon various factors, including size, shape, dispersion, and dielectric constant of solvent.[31] Powder X-ray diffraction pattern (Fig. 1b) shows peaks corresponding to face-centered-cubic (*fcc*) phase of Au (JCPDS Card No. 04-0784). The average crystallite size calculated by applying Scherrer equation to the most intense peak (111) was found to be 6 nm.

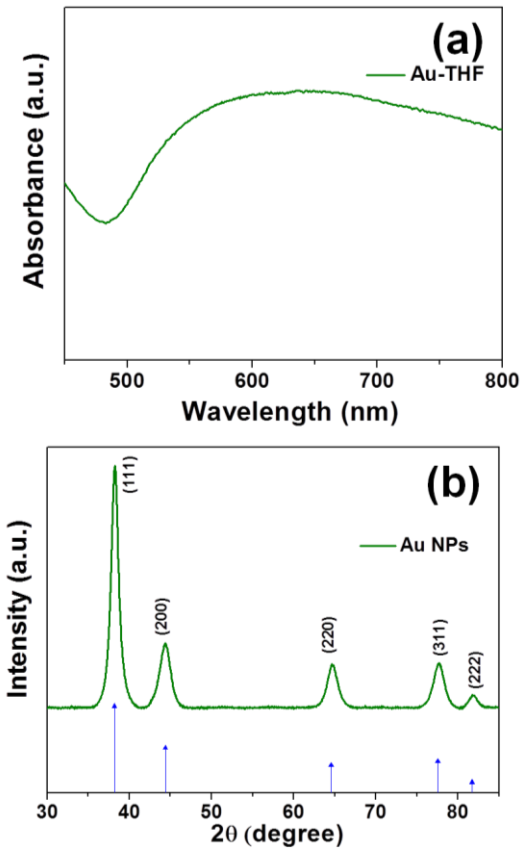

Fig. 1 Au nanoparticles (a) UV-visible spectrum; (b) powder X-ray diffraction pattern.

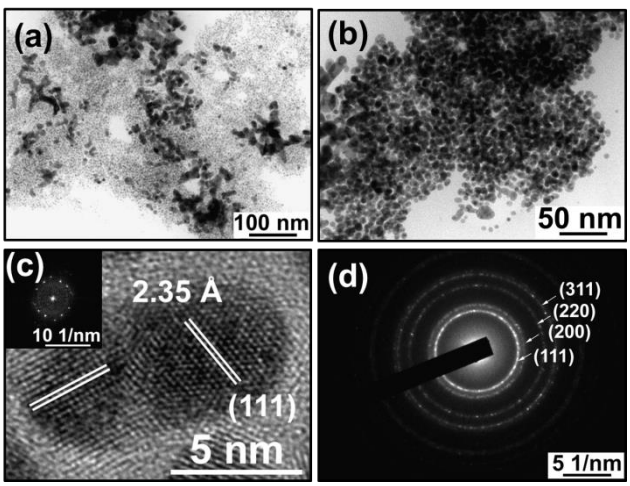

Fig. 2 Au nanoparticles: (a), (b) BFTEM images at two different magnifications (c) HRTEM image of representative Au nanoparticle (inset: FFT pattern); (d) SAED pattern corresponding to *fcc* Au.

Furthermore, the morphological characterization was carried out using TEM. The BFTEM image shows presence of aggregated particles which are mainly acircular in shape (Fig. 2a, b). The HRTEM image representative of an individual nanoparticle shows lattice fringes with *d* spacing of 2.35 Å corresponding to (111) plane of *fcc* Au (Fig. 2c). The SAED pattern exhibits ring pattern, confirming the polycrystalline nature of the sample; the pattern could be indexed to *fcc* phase of metallic Au (Fig. 2d). Thus, it could be inferred that in the absence of any surfactant or growth directing agent, Au-nanoparticles produced in THF are irregular in shape.[32]

2. Sn-nanoparticles synthesized in THF

The optical absorption spectrum of Sn-THF colloid is devoid of any band in visible region (see ESI) as reported in the literature for Sn nanoparticles.[33] The powder isolated from the colloid was subjected to XRD analysis, which showed the presence of tetragonal phase of Sn(0) (JCPDS Card No. 04-0673) (Fig. 3). The average crystallite size estimated by applying the Scherrer equation to the most intense (200) peak was 18 nm.

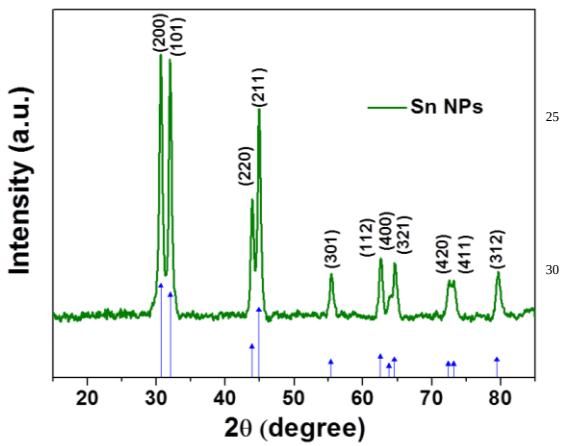

Fig. 3 Powder X-ray diffraction pattern of Sn nanoparticles.

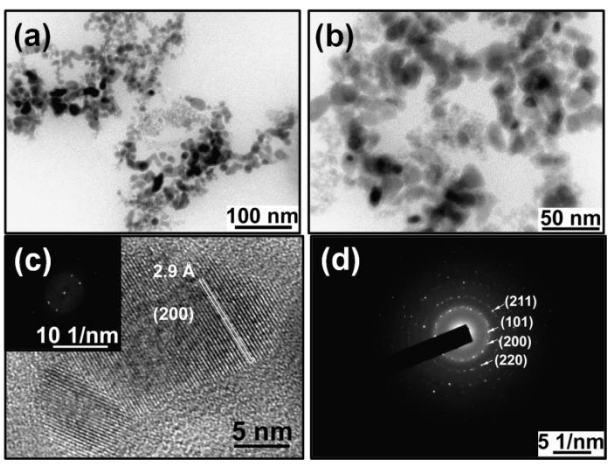

Fig. 4 Sn nanoparticles: (a), (b) BFTEM images at two different magnifications (c) HRTEM image of a representative Sn nanoparticle (inset: FFT pattern); (d) SAED pattern corresponding to tetragonal phase of Sn(0).

TEM characterization brought out the presence of aggregated nanostructures (Fig. 4a, b). The HRTEM image representative of a single nanoparticle shows lattice fringes with *d* spacing of 2.9 Å corresponding to the (200) plane (Fig. 4c) of tetragonal phase of Sn. The SAED shows ring pattern which could be indexed to Sn(0), thus corroborating PXRD data (Fig. 4d). We conclude that THF being a weak coordinating solvent cannot prevent aggregation of Sn nanoparticles due to the strong van der Waals forces of attraction among metal particles.[34]

3. Au_5Sn-AuSn nanocrystals

Benzyl alcohol, a high boiling solvent (b. p. 205 °C) was employed to facilitate the formation of Au-Sn intermetallic nanocrystals. The course of the reaction was followed by optical spectroscopy. The UV-visible absorption spectrum of the aliquot withdrawn prior to the reaction mixture being subjected to reflux conditions, exhibited a broad SPR band consistent with monometallic Au nanoparticles SPR band (Fig. 5a). As the reaction progressed the UV-visible spectrum was devoid of any SPR band (Fig. 5a). After 12 h, the reaction was stopped and the mixture was allowed to cool to room temperature. This was a preliminary indication of conversion of monometallic nanoparticles into intermetallic nanoparticles.

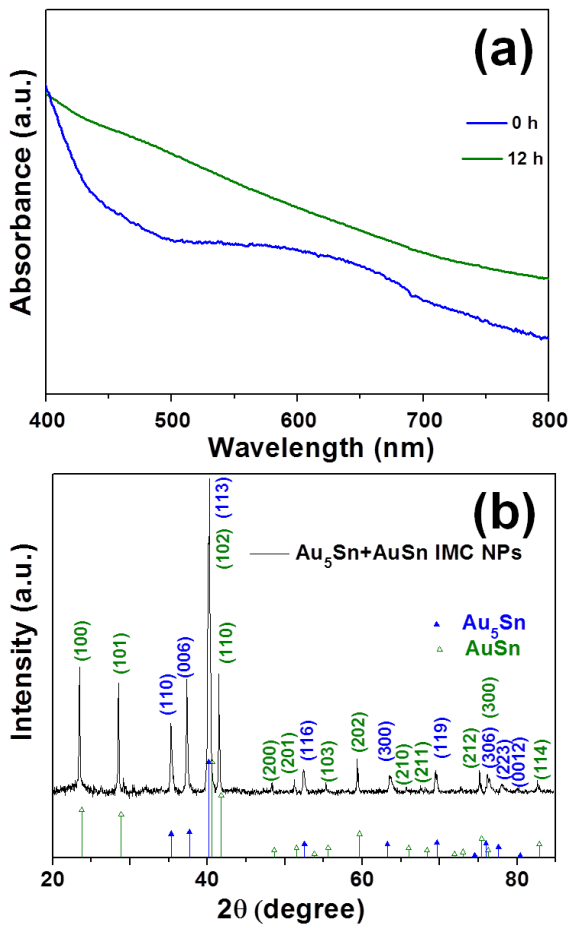

Fig. 5 Au_5Sn+AuSn intermetallic nanocrystals: (a) UV-visible spectra; (b) powder XRD pattern.

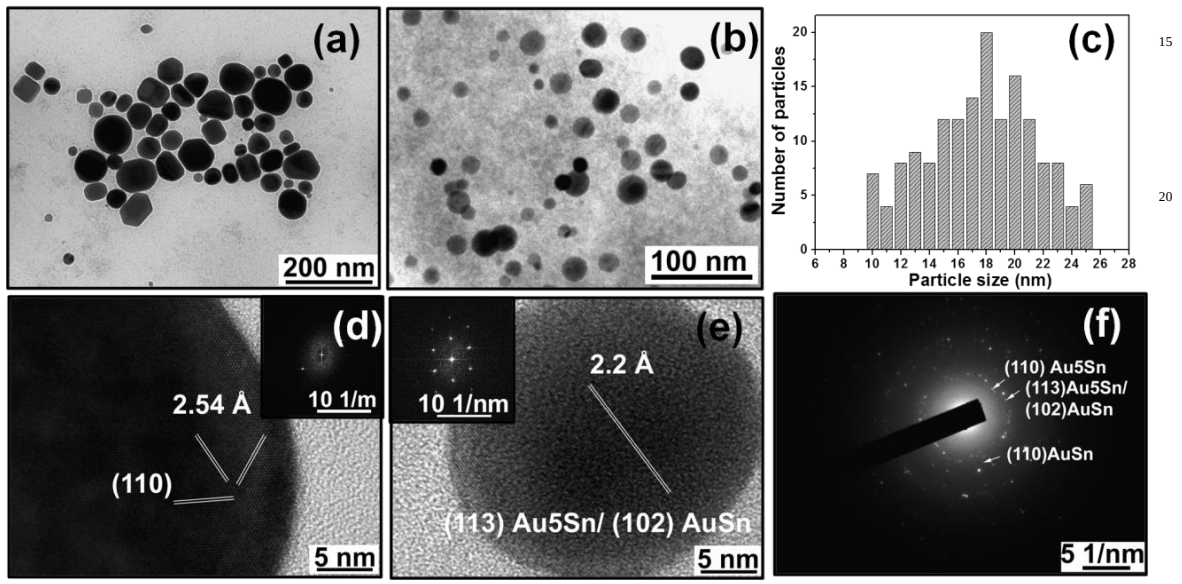

Fig. 6 Au_5Sn+AuSn intermetallic nanocrystals: (a), (b) BFTEM images; (c) histogram showing particle size distribution for spherical particles; (d), (e) HRTEM images of representative multifaceted and spherical nanocrystal (inset: FFT pattern); (f) electron diffraction pattern.

Optical absorption spectroscopy has been widely used to infer the formation of bimetallic nanostructures, including disordered alloys, core-shell, and intermetallic nanocrystals. In general, the core-shell nanostructures and a physical mixture comprising of segregated metal nanoparticles gives rise to two surface Plasmon absorption bands corresponding to individual metal species. For alloy nanoparticles, a single Plasmon absorption band positioned between the pure constituent nanoparticles is expected.[35] In case of intermetallic nanocrystals also known as "ordered alloys" the dampening of absorption band has been reported in literature.[11] In our case, Au is SPR active whereas, Sn does not show any band in the visible region; with course of reaction we noted complete disappearance of Au Plasmon absorption band. Similar observation has been made by Tabatabaei *et al.* wherein they noted dampening of the band of Au-Sn alloy nanoparticles in comparison to Au nanoparticles.[11] Structural characterization using PXRD has also been effectively used for the determination of intermetallic phase formation. Intermetallic exhibits a definite crystal lattice, which is different from its constituent monometallic counterparts. A well-defined PXRD pattern obtained from the reaction product (Fig. 5b) shows peaks corresponding to the rhombohedral Au_5Sn and hexagonal AuSn phases (JCPDS No. # 31-0568, 08-0463). No peak corresponding to segregated metallic phases was observable. This is in agreement with optical spectral studies wherein, absorption band due to Au completely disappeared.

The peaks of Au_5Sn phase were more intense than those of AuSn phase indicating that Au_5Sn could be a predominant phase. This observation is in accordance with the Au-Sn phase diagram which shows 68 wt% Au_5Sn and 32% AuSn in Au-rich, eutectic Au/Sn alloy.[13] The Au–Sn phase diagram suggests that the two phases, AuSn and Au_5Sn may co-exist in the range of 15–50% Sn.[18] Moreover, the as-prepared nanostructures are well crystalline, thus require no post-synthesis processing.

The sample was further examined by transmission electron microscopy (TEM). The BFTEM micrographs show the presence of well-dispersed spherical nanocrystals along with multifaceted nanocrystals mainly comprising hexagons and octahedra (Fig. 6a, b). The average diameter of spherical nanocrystals, calculated manually by constructing a histogram was found to be 19 nm (Fig. 6c). The HRTEM image representative of a single nanoparticle displayed lattice fringes with *d* spacing of 2.54 Å corresponding to (110) plane of rhombohedral phase of Au_5Sn (Fig. 6d). On the other hand, HRTEM image of a spherical particle (Fig. 6e) showed lattice fringes with *d* spacing of 2.2 Å that could be assigned either to (113) plane of rhombohedral Au_5Sn phase or (102) plane of hexagonal AuSn phase, as both the planes display 100% intensity for respective phases. The SAED pattern shows ring pattern with bright spots confirming the well crystalline nature of the sample (Fig. 6f) and the pattern could be indexed to both Au_5Sn and AuSn phases, thus corroborating the XRD results.

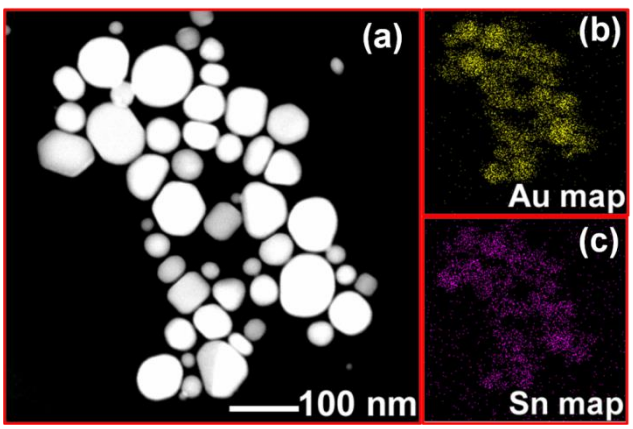

Fig. 7 Area mapping of Au_5Sn+AuSn nanocrystals (a) STEM dark field image; (b) Au map; (c) Sn map.

To get an insight into the dispersion of the Au_5Sn and AuSn intermetallic phases in Au-Sn physical mixture with their atomic distributions, EDS mapping was performed in STEM mode. STEM-Dark field (STEM-DF) image (Fig. 7a) taken from multifaceted particles shows a difference in contrast of individual nanocrystals. The nanocrystals with brighter contrast correspond to Au_5Sn whereas the ones with darker contrast are those of AuSn since the intensity is directly proportional to the square of the atomic number of the constituent elements. The presence of two different phases in the sample was further substantiated by the corresponding EDS analysis (Fig. 7b, c). In another STEM-DF image (see ESI) where mainly spheres and hexagons were present, the point EDS spectrum from a single hexagonal nanoparticle shows the presence of Au and Sn in the ratio of approximately 1:1 whereas, EDS spectrum obtained from a single spherical nanoparticle confirms the ratio of Au:Sn as ~5:1. The formation of two different phases was further validated from the contrast in STEM-DF image and the corresponding mapping images (see ESI).

4. AuSn intermetallic nanocrystals

When we reacted Au:Sn in a stoichiometry of 1:1, nucleation of both the phases Au_5Sn and AuSn takes place together in the system. This was found to take place quite reproducibly. Within the detection limit of X-ray diffractometer no peaks corresponding to pure metal (Au or Sn) were present. This observation though unusual, was not surprising. Cable and Schaak reported the synthesis of phase pure Au_5Sn intermetallic compound using polyol process with a Au:Sn reaction ratio of 1:1 at 175 °C.[8a] We also performed the reaction at lower temperature (165 °C) with overall stoichiometry of Au:Sn at 1:1, however we still obtained the Au_5Sn+AuSn phase mixture. Therefore, in order to realize phase pure intermetallic of Au-Sn system, we optimized an appropriate ratio of 1:2 of Au:Sn which led to the formation of phase pure AuSn. AuSn is the only congruently melting phase in Au-Sn phase diagram.[36] The UV-visible absorption spectrum reveals the absence of absorption band of Au and the PXRD pattern shows intense peaks, perfectly matching with hexagonal phase of AuSn (space group P63/mmc) (JCPDS card No. 08-0463). To within the detection limit of XRD, no peak corresponding to a different polymorph of Au-Sn is present in the sample (Fig. 8). In addition, the DSC profile of AuSn intermetallic nanocrystals (see ESI) shows the presence of a single endothermic peak at 409 °C, which is indeed lower than the bulk AuSn phase (melting point = 419.3 °C).[14] Absence of any other endothermic peak despite using higher concentration of Sn for the realization of phase pure AuSn, further confirms its phase purity and homogeneity.

The BFTEM micrograph shows predominantly the presence of well-defined hexagonal nanocrystals along with a few spherical nanoparticles (Fig. 9a, b). The crystallinity was further confirmed with a high resolution TEM. The HRTEM micrograph features lattice fringes with *d* spacing of 2.2 Å and 3.74 Å corresponding to (102) and (100) planes of hexagonal AuSn phase, respectively (Fig. 9c). The lattice fringes in high resolution TEM micrographs evidences that the nanoparticles are mostly single crystalline. The electron diffraction pattern confirms the formation of phase pure hexagonal AuSn structure, thus correlating with PXRD results (Fig. 9d).

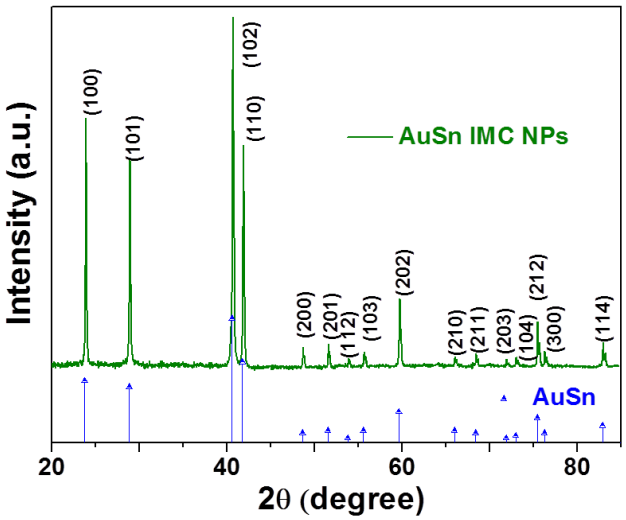

Fig. 8 Powder XRD pattern of AuSn intermetallic nanocrystals.

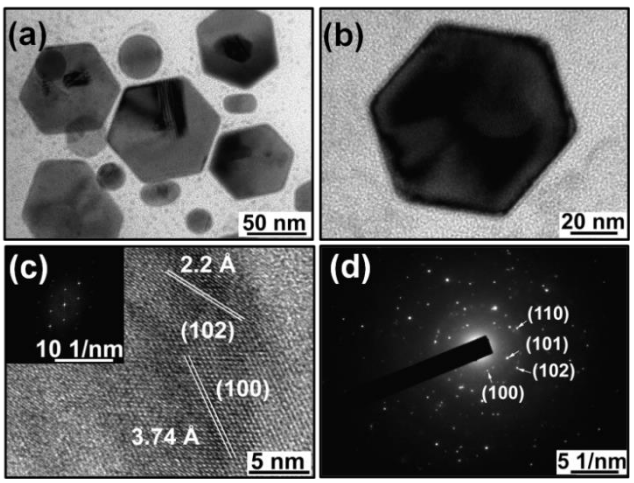

Fig. 9 AuSn intermetallic nanocrystals: (a), (b) BFTEM image at two different magnifications; (c) HRTEM image of a representative AuSn nanocrystal (inset: FFT pattern); (d) Electron diffraction pattern indexed to hexagonal phase of AuSn.

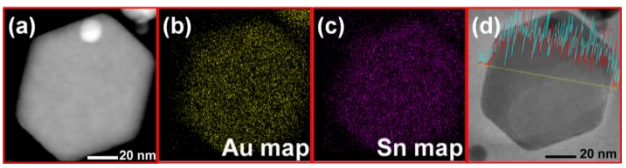

Fig. 10 Area mapping of hexagonal AuSn nanocrystal (a) STEM dark field image; (b) Au map; (c) Sn map; (d) Line spectra; Au (red trace), Sn (cyan trace).

Fig. 10a shows STEM-DF image and corresponding EDS mapping of a representative single hexagon AuSn particle (Fig. 10b, c). EDS mapping gives direct evidence of homogeneous distribution of constituent metals Au and Sn throughout the dimension of AuSn intermetallic nanocrystal. Furthermore, composition and homogeneity was confirmed from the

corresponding line scan and EDS spectrum obtained from an individual AuSn hexagonal nanoparticle (Fig. 10d).

5. Au_5Sn intermetallic nanocrystals

Optimization of stoichiometry of Au:Sn was found to be a crucial parameter in achieving phase pure Au-rich Au-Sn intermetallics with controlled morphology. The UV-visible absorption spectrum is devoid of Au Plasmon band suggesting the completion of reaction. The powder XRD pattern recorded for the isolated powder shows the formation of phase pure rhombohedral Au_5Sn (Space group R3) (JCPDSNo# 31-0568) (Fig. 11). No peaks corresponding to Au, Sn, or other intermetallics present in Au-Sn system were observed in the PXRD pattern suggesting successful synthesis of desired intermetallic nanoparticles. In addition, intense peaks indicate that the sample is well crystalline.

The powder sample was further examined by TEM. The BFTEM micrographs reveal the presence of distinct and well separated spherical particles with an average diameter of 12 nm (Fig. 12a, b). The HRTEM image of individual nanocrystals displays lattice fringes with *d* spacing of 2.54 Å which is consistent with the (110) plane of rhombohedral phase of Au_5Sn (Fig. 12c). The SAED pattern could be indexed to Au_5Sn intermetallic phase, thus correlating with PXRD results (Fig. 12d). The EDS spectra obtained from several nanocrystals shows a stoichiometry of the constituent metals, Au and Sn in the ratio of approximately 5:1 (see ESI). The corresponding Au and Sn maps reveal a homogeneous distribution of elements in Au_5Sn nanocrystals. (Fig. 13a, b, c) and EDS line spectra measured across a single nanocrystal measuring about 10 nm further validated the composition of Au_5Sn intermetallic (Fig. 13d).

Achieving the formation of intermetallic compounds by carrying out reactions with different stoichiometries have been reported in literature.[21,38] For example, phase pure PtSn intermetallic nanocrystals were realized by employing 1:8 Pt:$SnCl_2$ molar ratio.[39] It was reasoned that excess Sn metal is oxidized and remains in solution as small dispersed nanoparticles. Similarly, $FeSn_2$ and Co_3Sn_2 intermetallic phases were formed only with large excess of Sn which forms an oxide shell.[8a] However, in our case, we surmise that extra Sn is leached out after washing the product with methanol. We do not observe any core-shell architecture for our intermetallic nanocrystals; in addition, point EDS spectra and mapping of several different nanocrystals performed under STEM mode yields the formation of pure intermetallic compounds in appropriate stoichiometry. Au_5Sn has been reported to form after protracted interdiffusion at room temperature in very Au-rich film couples or upon high-temperature annealing.[36] Recently, Au_5Sn formation has been observed in electrodeposited Au/Sn couples at room temperature.[37] Herein, phase pure Au_5Sn intermetallic was achieved in gold rich ambience in solution.

Discussion about interatomic diffusion, plausible mechanism

In addition to Au_5Sn+AuSn phase mixture, we obtained phase pure nanocrystals of AuSn and Au_5Sn intermetallics. Although such systems are well studied however, solution based synthesis as illustrated above remains unprecedented. In order to have an understanding of our approach, we took note of the important processes, such as "interatomic diffusion" and "digestive ripening" which are taking placing simultaneously and eventually dictating the formation of nanocrystals.

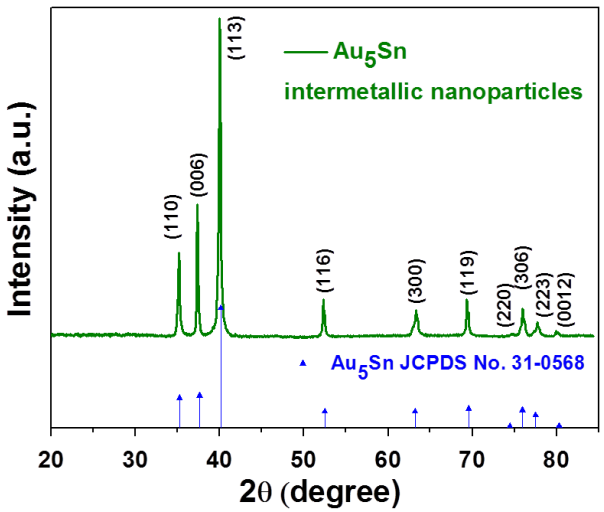

Fig. 11 Powder XRD pattern of Au_5Sn intermetallic nanocrystals.

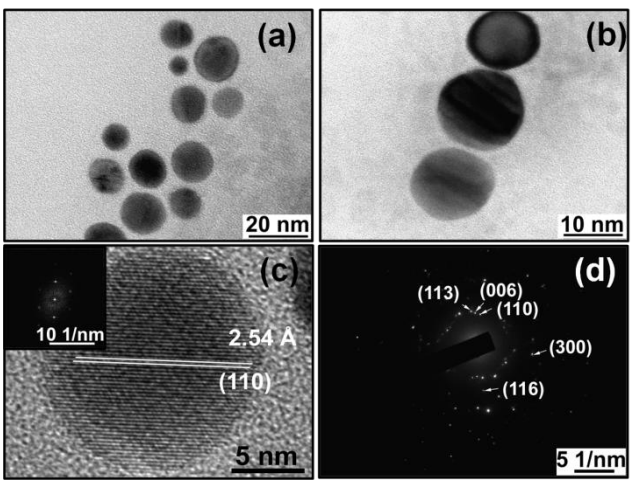

Fig. 12 Au_5Sn intermetallic nanocrystals: (a), (b) BFTEM image at two different magnifications; (c) HRTEM image of a representative Au_5Sn nanocrystal (inset: FFT pattern); (d) electron diffraction pattern indexed to rhombohedral phase of Au_5Sn.

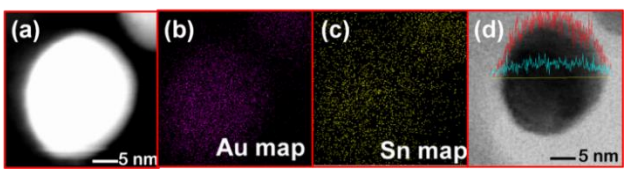

Fig. 13 Area mapping of hexagonal Au_5Sn nanocrystal: (a) STEM dark field image; (b) Au map; (c) Sn map; (d) line spectra; Au (red trace), Sn (cyan trace).

The process of interatomic diffusion at nanosize regime leads to ordered alloy formation. This is due to the increase in reaction

kinetics in the form of diffusion rates, thus rate of mixing gets enhanced in the presence of vacancy defect at the boundary between the two nanoparticles.[40,41,42] We took the strategic advantage of selecting Au-Sn system, which is an intriguing system to study the interatomic diffusion process as it is expected to take place at relatively lower temperature.[43] Dyson studied the diffusion of gold in tin single crystals in the temperature range of 135-225 °C using a radioactive tracer technique.[43] Mostly, the diffusivity of Au into Sn is more rapid and proceeds by interstitial mechanism. The diffusivity of Sn into Au is considerably less and takes place by substitution mechanism.

It is well known that "Digestive Ripening" process in contrast to the "Ostwald Ripening" process[44] leads to the formation of well-formed monodisperse intermetallic nanocrystals. Initially, the reaction was performed with HDA as a capping agent which was employed successfully for the synthesis of monodisperse nanoparticles.[24] However, in case of Au-Sn system, the nanoparticles are not well formed and are largely aggregated which could be attributed to the weak binding nature of HDA. Therefore, to achieve well formed nanocrystals a combination of benzyl alcohol and TOPO and TOP was chosen. Benzyl alcohol was selected since it is a high boiling solvent and it could facilitate the formation of Au-Sn intermetallic nanocrystals. Benzyl alcohol is benign in nature and has been extensively investigated as a non-aqueous solvent towards the synthesis of various kinds of nanomaterials.[45] TOPO and TOP, efficient digestive ripening and growth directing agents have been reported as versatile ligands for size and shape controlled synthesis of various nanoparticles.[46] So far, by replacing the HDA/THF with TOPO/TOP/BA, well formed nanocrystals of AuSn + Au_5Sn have been realized.

The molar amounts of metal nanoparticle precursor had to be optimized and prudently controlled in realizing phase pure Au_5Sn and AuSn intermetallic nanocrystals. It is very intriguing to note that in the same Au-Sn system, two different phase pure intermetallics can be realized by optimizing molar amounts of metal nanoparticle precursors. To date, Au_5Sn, AuSn, and mixture of two phases have been synthesized in single solution in only thin film form by altering the deposition current density. Our observation of realizing them as well-formed nanocrystals is unprecedented. In literature, Cable and Schaak have demonstrated that the multiple phase-pure intermetallics can be realized for Co-Sb by controlling initial metal concentration and reaction temperature. They further showed that two distinct crystalline phases for Cu-Sn and Co-Sn system can form in a single reaction as a function of temperature.[8a]

The driving force for our reaction involves two steps: (a) top down process wherein dissolution of Au and Sn nanoparticles takes place and digestive ripening agents act as labile metal atom carriers by removing and transplanting atoms from one particle to another and (b) bottom up process in which nucleation of homogeneous intermetallic phases of Au-Sn system takes place *via* interatomic diffusion of atoms of the constituent elements in the nanosize regime. Such a reaction is thermodynamically feasible, i.e., the bond dissociation energy of Au-Sn is comparatively higher than either of Au-Au or Sn-Sn bond[47] (Table 1). Similar strategy has been demonstrated by Klabunde's group by carrying out successful synthesis of alloy systems in gram quantities at low temperature.[27]

Table 1. Bond dissociation energies in diatomic molecules.

Bond	Bond dissociation energy (kJ/mol)
Au-Au	226.2 ± 0.5
Au-Sn	256.5 ±7.2
Sn-Sn	187.1 ± 0.3

Conclusions

In summary, we synthesized Au-rich Au-Sn intermetallic nanocrystals with tuned morphology and phase using solution based approach. The compositions and phase formations have been established by powder X-ray diffraction, TEM, HRTEM, STEM and EDS analysis. The transformation of monometallic nanoparticles into intermetallic nanocrystals is a diffusion based process driven by digestive ripening. Careful selection of solvent, stoichiometry and growth directing agents is an important pre-requisite for establishing distinct phases of Au-Sn system with controlled morphology. We envisage that by varying the thermodynamic parameters such as temperature, stoichiometry, and understanding inter-diffusion of constituent metals, nanoscaled alloys or core-shell structures could also be realized. Efforts in this direction are in progress in our laboratories.

Experimental Section

Materials: Gold foil (99.95 % metal basis) was purchased from Arora Matthey Limited. Tin foil (99.998% metal basis), tri-*n*-octylphosphine (TOP, 90% technical grade), and tri-*n*-octyl phosphine oxide (TOPO, 90% technical grade) were purchased from Sigma Aldrich. Tungsten crucibles were obtained from R. D. Mathis Company, California. Tetrahydrofuran (S. D. Fine Chemicals Limited, India) was dried over sodium-benzophenone and degassed by several freeze–pump–thaw cycles. Methanol (HPLC grade, 99.9%) was dried over magnesium methoxide and distilled prior to use. Benzyl alcohol (S. D. Fine Chemicals Limited, India), of analytical grade, was used in the synthesis as received. All glassware were thoroughly dried in a hot air oven (120 °C) and evacuated just prior to use. All reactions were carried out under an Ar atmosphere using standard Schlenk techniques.

Synthesis of Au/Sn-THF nanopowder

Colloids of Au and Sn nanoparticles in THF solvent were prepared by the solvated metal atom dispersion (SMAD) method similar to our previous reports.[30] Briefly, in a typical experiment, 50 mg of metal (Au/Sn) was placed in the alumina coated tungsten crucible which was cured prior to the experiment to ensure removal of moisture and other volatile impurities. A solvent Schlenk tube containing dried and degassed THF solvent was connected to the SMAD reactor through a bridge-head and the entire reaction chamber was evacuated to 1-2 x 10^{-3} mbar. Once this pressure was attained, 20 mL of solvent was condensed on the walls of the reactor which were cooled using a liquid N_2 bath. The crucible was heated resistively until metal vaporization began, which was apparent by the appearance of violet color and red color on a white matrix, respectively for Au and Sn

experiments. The co-condensation of metal atoms with solvent vapor was continued for a period of 2 h in which the color of the matrix deepened to violet-red/ dark-red (Au/Sn). The pressure of 1-2 x 10^{-3} mbar was maintained throughout the experiment. An additional 20 mL of solvent was condensed and the reaction mixture was allowed to warm up slowly under an argon atmosphere. The colloids obtained were stirred in the reactor under argon for 10 min and finally siphoned into a Schlenk tube. THF as a coordinating solvent produced stable dark violet and black colored colloids, respectively, for Au and Sn. The powders were isolated by applying dynamic vacuum.

Synthesis of Au-Sn intermetallic nanocrystals

The synthesis of Au-Sn intermetallic nanocrystals was performed by the following method. Au and Sn nanopowders (as-obtained by SMAD method) in an appropriate stoichiometric ratio (Table 2), tri-*n*-octyl phosphine and tri-*n*-octyl phosphine oxide (M: TOPO: TOP~ 1: 1: 20: 20) were dispersed in 30 mL of benzyl alcohol by sonicating for 5 min in a 100 mL two-necked round-bottom flask equipped with a water cooled condenser. This solution was stirred vigorously under bubbling Ar for a few minutes. The reaction mixture was brought to reflux using a sand bath under an argon blanket and magnetic stirring. The temperature (200 °C) was held constant for a period of 12 h. The progress of the reaction was monitored by taking aliquots (1 mL) at regular intervals of time for optical characterization. The color of the colloid gradually turned from black to light brown. The reaction mixture was allowed to cool to room temperature and nanocrystals were purified with anhydrous methanol. The precipitate was isolated by centrifuging at 3000 rpm and subsequently washed thrice with methanol to remove excess capping agent, followed by drying under ambient conditions.

Table 2. Summary of experimental conditions optimized for the synthesis of different Au-Sn nanocrystals and their morphology obtained.

Au:Sn molar ratio	Temperature (°C)/time (h)	Phase obtained	Morphology
1:1	200/12	Au_5Sn+AuSn	Multifaceted + spherical
2:1	200/12	Au_5Sn	Spherical
1:2	200/12	AuSn	Mainly hexagons + spherical

Measurements

UV-visible Spectroscopy

Optical absorption data were collected at room temperature using a Perkin Elmer Lambda 700 UV-vis-near-IR spectrophotometer with a double monochromator.

Powder X-ray diffraction (PXRD)

Powder X-ray diffraction data were collected on a Bruker D8 Advance X-ray diffractometer equipped with a graphite monochromator using Cu K_α (0.154 nm) radiation, at a scanning rate of 0.2° min^{-1}.

Transmission Electron Microscopy (TEM)

The bright-field transmission electron microscopy images (BFTEM), high resolution electron microscopy (HRTEM) images, selected area electron diffraction (SAED) patterns, energy-dispersive-X-ray spectroscopy (EDS), and Scanning transmission electron microscopy-elemental mapping (STEM-EDS) images of nanocrystals were collected using a JEOL JEM-2100F microscope operating at an accelerating voltage of 200 kV, equipped with an Oxford energy-dispersive X-ray (EDX) detector. The TEM specimens were prepared by slow evaporation of diluted colloids, obtained by dispersion of powders in THF, deposited on Formvar coated copper grid.

Differential scanning calorimeter (DSC)

The melting points of AuSn and Sn nanopowders were determined by a differential scanning calorimeter (METTLER-TOLEDO DSC1) under a flow of N_2 atmosphere at a heating rate of 5 °C/min, from room temperature to ~450 °C.

Acknowledgements

We gratefully acknowledge financial support from the Council of Scientific & Industrial Research, India. We also thank the Indian Institute of Science for funding the procurement of a 200 kV TEM and the Institute XRD facility for the powder XRD data. N.A. thanks the CSIR for a fellowship.

Notes and references

[a] *Department of Inorganic & Physical Chemistry, Indian Institute of Science, Bangalore 560 012, India. Fax: +91-80-2360 1552; Tel: +91-80-2293 2825; E-mail: jagirdar@ipc.iisc.ernet.in*

† Electronic Supplementary Information (ESI) available: UV-vis spectrum of Sn nanoparticles, STEM-EDS mapping for Au_5Sn+AuSn phase mixture nanocrystals,and EDS spectrum for Au_5Sn intermetallic nanocrystals. DSC profiles of AuSn and Sn nanopowders. See DOI: 10.1039/b000000x/

1 G. Gschneidner,A. Russell, A. Pecharsky, J. Morris, Z. Zhang, T. Lograsso, D. Hsu, C. Lo and D. Kesse, *Nat. Mater.* ,2003, **2**, 587.
2 C. Roychowdhury, F. Matsumoto, V. B. Zeldovich, S. C. Warren, P. F. Mutolo, M. Ballesteros, U. Wiesner, H. D. Abruña and F. J. DiSalvo, *Chem. Mater*., 2006, **18**, 3365.
3 L. Shao, W. Zhang, M. Armbrster, D. Teschner, F. Girgsdies, B. Zhang, O. Timpe, M. Friedrich, R. Schlçogl and D. S. Su, *Angew. Chem. Int. Ed*., 2011, **50**, 10231.
4 C. M. Tsai, W. C. Luo, C. W. Chang, Y. C. Shieh and C. R. Kao, *J. Elec. Mater*., 2004, **33**, 1424.
5 H. Shao, H. Xu, Y. Wangand X. Li, *Nanotechnology*, 2004, **15**, 269.
6 N. H. Chou and R. E. Schaak, *J. Am. Chem. Soc*., 2007, **129**, 7339.
7 V. Nandwana, K. E. Elkins, N. Poudyal, G. S. Chaubey, K. Yano and J. P. Liu, *J. Phy. Chem. C*, 2007, **111**, 4185.
8 *(a)*R. E. Cable and R. E. Schaak, *Chem. Mater*., 2005, **17**, 6835; *(b)* R. E. Schaak, A. K. Sra, B. M. Leonard, R. E. Cable, J. C. Bauer, Y.-F. Han, J. Means, W. Teizer, Y. Vasquez and E. S. Funck, *J. Am. Chem. Soc*., 2005, **127**, 3506.
9 L.-Y. Hsiao and J.-G. Duh, *J. Electrochem. Soc.*, 2005, **152**, J105.
10 D. G.Ivey, *Micron*, 1998, **29**, 281.
11 S. Tabatabaei, A. Kumar, H. Ardebili, P. J. Loos and P. M. Ajayan, *Microelectronics Reliability*,2012, **52**, 2685.
12 P. Buffat and J. P. Borel, *Phys. Rev. A*,1976, **13**, 2287.
13 H. Okamoto and T. B. Massalski, *Phase diagrams of binary gold alloys*; ASM International: Metals Park, Ohio, 1987.

14 G. S. Matijasevic, C. C. Lee and C. Y. Wang, *Thin Solid Films*, 1993, **223**, 276.
15 K. Osada, S. Yamaguchi and M. Hirabayashi, *Trans. Jpn. Inst. Met.*,1974,**15**, 256.
16 J. P. Jan, W. B. Pearson, A. Kjekshus and S. B. Woods, *Can. J. Phys.*,1963, **41**, 2252.
17 W. Tang, A. He, Q. Liu and D. G. Ivey, *J Mater Sci: Mater Electron.*, 2008, **19**, 1176.
18 E. Djurfors and D. G. Ivey, *J. Electron. Mater*., 2001, **30**, 1249.
19 J. -G. Wang, M. -L.Tian, T. E. Mallouk and M. H. W. Chan, *Nano Lett.*, 2004, **4**, 1313.
20 K. Yu, Z. Wu, Q. Zhao, B. Li and Y.Xie, *J. Phys. Chem. C* 2008, **112**, 2244.
21 F. Dawood, B. M. Leonard and R. E. Schaak, *Chem. Mater.*, 2007, **19**, 4545.
22 N. H. Chou and R. E. Schaak, *Chem. Mater.*, 2008, **20**, 2081.
23 *(a)* X.M. Lin, C. M. Sorensen and K. J. Klabunde, *J. Nanopart. Res*., 2000, **2**, 157; *(b)* K. J. Klabunde, C. M. Sorensen, S. I. Stoeva, B. L. V. Prasad, A. B. Smetana and X. M. Lin, in *Metal Nanoclusters in Catalysis and Materials Science: the Issue of Size Control, Part II Methodologies*, ed. C. Corrain, G. Schmid and N. Toshima, Elsevier Science, Amsterdam, 2008, ch. 11, pp. 233–252.
24 N. Arora and B. R. Jagirdar, *J. Mater. Chem.*, 2012, **22**, 20671.
25 S. Cingarapu, Z. Yang, C. M. Sorensen and K. J. Klabunde, *Chem. Mater*., 2009, **21**, 1248.
26 S. B. Kalidindi and B. R. Jagirdar, *J. Phys. Chem. C*, 2008, **112**, 4042.
27 A. B. Smetana, K. J. Klabunde, C. M. Sorensen, A. A. Ponce and B. Mwale, *J. Phys. Chem. B*, 2006, **110**, 2155.
28 Manuscript submitted.
29 K. J. Klabunde, P. L. Timms, P. S. Skell and S. Ittel, *Inorg. Synth.*, 1979, **19**, 59.
30 N. Arora and B. R. Jagirdar, *J. Mater. Chem.*, 2012, **22**, 9058.
31 S. Link and M. A. El-Sayed, *J. Phys. Chem. B*, 1999, **103**, 4212.
32 S. Stoeva, K. J. Klabunde, C. M. Sorensen and I. Dragieva, *J. Am. Chem. Soc*., 2002, **124**, 2305**.**
33 M. Noh, Y. Kim, M. G. Kim, H. Lee, H. Kim, Y. Kwon, Y. Lee and J. Cho, *Chem. Mater*., 2005, **17**, 3320.
34 G. A. Held, G. Grinstein, H. Doyle, S. Sun and C. B. Murray, *Phys. Rev. B*, 2001, **64**, 012408.
35 S. Link, Z. L. Wang and M. A. El-Sayed, *J. Phys. Chem. B*,1999, **103**, 3529.
36 L. Buene, H. Falkenberg-Arell, J. Gjønnes and J.Taftø, *Thin Solid Films*, 1980, **67**, 95.
37 W. Tang, A. He, Q. Liu and D. G. Ivey, *Acta Materialia*, 2008, **56**, 5818.
38 *(a)* H. Abe, F. Matsumoto, L. R. Alden, S. C. Warren, H. D. Abruña and F. J. Di Salvo, *J. Am. Chem. Soc.*, 2008, **130**, 5452; *(b)* D. D. Vaughin and R. E. Schaak, *J. Alloys Compd.*,2010, **490**, 98.
39 J. C. Bauer, X. Chen, Q. Liu, T.-H. Phan and R. E. Schaak, *J. Mater. Chem.*,2008, **18**, 275.
40 K. Yu,T. Yao,Z. Pan, S. Wei and Y. Xie, *Dalton Trans.*, 2009, 10353.
41 T. Shibata, B. A. Bunker, Z. Zhang, D. Meisel, C. F. Vardeman and J. D. Gezelter, *J. Am. Chem. Soc*., 2002, **124**, 11989.
42 H. Mori and H.Yasuda, *Mater. Sci. Eng., A*,2001, **312**, 99.
43 *(a)* B. F. Dyson, *J. Appl. Phys.*,1966, **37,** 2375; *(b)* B. F. Dyson, T. R. Anthony and D. Turnbull, *J. Appl. Phys.*,1967, **38**, 3408.
44 F. Griffin and D. Fitzmaurice, *Langmuir*, 2007, **23**, 10262.
45 *(a)* M. Niederberger, M. H. Bartl and G. D. Stucky, *J. Am. Chem. Soc.*,2002, **124,** 13642;*(b)* M. Niederberger, N. Pinna, J. Polleux and M. Antonietti, *Angew. Chem. Int. Ed.*,2004, **43**, 2270.
46 C. B. Murray, D. J. Norris and M. G. Bawendi *J. Am. Chem. Soc.*,1993, **115**, 8706.
47 D. R. Lide, *CRC Handbook of Chemistry and Physics*, 90th ed.; CRC Press: Boca Raton, 2010.